Archives of Materials Science and Engineering

Volume 126
Issue 1
March 2024
Pages 5-14

International Scientific Journal
published monthly by the
World Academy of Materials
and Manufacturing Engineering

DOI: 10.5604/01.3001.0054.6778

Effect of fatigue behaviour on fracture in the 4th gear of a pick-up truck

P. Janmanee, R. Saodaen, C. Thanadngarn, T. Kumnorkaew, K. Jamkamon, K. Utjimajiratthitikarn *

Mechanical and Industrial Engineering Department, Faculty of Engineering, Rajamangala University of Technology Krungthep (RMUTK), 2 Nanglin Chi Road, Sathorn, Bangkok 10120, Thailand

* Corresponding e-mail address: kajorn.de63@mail.rmutk.ac.th

ORCID identifier: https://orcid.org/0009-0007-8246-1669 (K.U.)

ABSTRACT

Purpose: This paper aims to investigate the effect of fatigue behaviour on fracture in the 4th gear (helical gear) of a pick-up truck.

Design/methodology/approach: Fracture on the failed helical gear is characterised through metallographic and fractographic analyses. Mechanical testing and finite element simulation are employed to assess the factors contributing to the gear failure.

Findings: The microstructure observed in the case layer was martensite, leading to a hard and brittle surface due to carburising. Failure initiated at the crack origins and then propagated to the instant fracture zone in the core of the gear tooth. Multiple crack origins accelerated the development of ratchet marks, attributed to the high intensity of stress exerted on the workpiece and ultimately leading to a substantial final overload zone. Hardness decreased with increasing depth of the gear surface due to the effects of carburising and hardening treatments. Stress was initiated from the contact stress on the gear tooth surface and transformed into bending stress along the central axis of the gear. The contact stresses became critical when the torque surpassed the contact strength of the material.

Research limitations/implications: Simulation samples must be experimentally validated to improve the results.

Practical implications: Metallographic and fractographic analyses are crucial in elucidating the wear mechanisms in mechanical components. Additionally, finite element analysis can indicate the influence of stress on the mechanical part, providing insights that can effectively guide the limiting transmission power to ensure extended service life.

Originality/value: Cost reduction, time for analysis, and finding the root causes of the problem should be conducted to improve the implementation process, leading to high product quality.

Keywords: Helical gear, Gear failure, Finite element

Reference to this paper should be given in the following way:

P. Janmanee, R. Saodaen, C. Thanadngarn, T. Kumnorkaew, K. Jamkamon, K. Utjimajiratthitikarn, Effect of fatigue behaviour on fracture in the 4th gear of a pick-up truck, Archives of Materials Science and Engineering 126/1 (2024) 5-14. DOI: https://doi.org/10.5604/01.3001.0054.6778

PROPERTIES

1. Introduction

Helical gear is one of the most common gear types in automobiles. The gear function transmits power and motion from one parallel shaft to another. It is a key transmission system component thanks to its high contact ratio with smooth rotation. In various applications, the helical gears support the reverse and alternating rotations; therefore, the gears must be strong and durable. However, failures caused by continuous operation are inevitable, subsequently causing severe effects on safety, including life and assets. It is recognised that vehicle components, particularly those in trucks, frequently function under conditions of substantial load and, in numerous instances, must continue operating without the benefit of regular inspections. The failure of a component may result in the component being damaged before its designed lifespan [1]. The simulation model with a software program is possibly used to identify the root cause of the failure of the vehicle part in order to limit working operation or identify service life [2-3].

Generally, there are several root causes for gear failure: improper design [4]; improper selection of materials and production processes [5,6]; misalignment as a result of elastic deformation, manufacturing errors, or assembly errors [7-9]; contact repetition between components, which leads to pitting or scuffing on the gear surface [10]; bending of the gear tooth [11]; incorrect maintenance [12,13]; failure caused by practical application, e.g., high bending stress acting on the gear tooth during cyclic loading [14]; hardness of the gear surface [15]. Generally, stresses related to a number of cycles (S-N curve) can be used to identify the maximum load where the failure in the gear is found [16].

Nevertheless, the majority of studies concerning the failure of components and mechanical frameworks remain relatively inaccessible within the realm of academic literature. Concurrently, disseminating case studies is crucial in mitigating failures and enhancing the designs of contemporary production methodologies.

The aforementioned factors have frequently been identified through analysis of previous studies. One of the primary reasons for the failure of rear differential gears is attributable to damage and fractures. Furthermore, fatigue frequently emerges as a prevalent form of deterioration under normal operating conditions, where the stress fluctuating is below the threshold that causes damage. Fatigue-related damage typically originates in critical areas, where defects related to structure, materials, and manufacturing processes converge, thereby significantly influencing the lifespan of gears from these zones. In an instance involving a vehicle travelling at a speed of 90 km/h and experiencing gearbox noise. The accident during the operation of the vehicle may have severe effects on safety, including life and assets. More damage to the gearbox commonly occurred on gear 4th, as shown in Figure 1. Therefore, this study aims to investigate the damage to a helical gear within the gearbox. The pick-up truck has a power of 144 HP. The results of this study will elucidate both the damage mechanism and its underlying causes. The data obtained from this analysis will contribute to vehicle maintenance strategies, with the research outcomes offering a foundation for recommendations and enhancements to improve vehicle reliability.

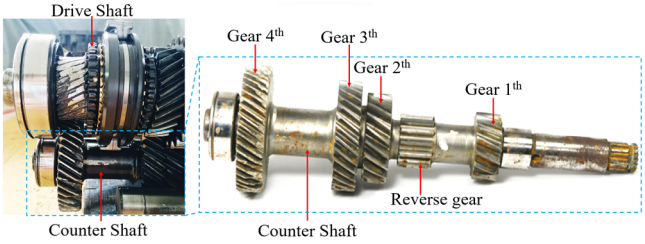

Fig. 1. Locations of cracks on the 4th gear in the countershaft

2. Experimental procedure

In this research, two approaches involving material characterisation and mechanical testing were carried out. Details are as follows.

2.1. Material characterisation

The investigation was conducted on a failed helical gear made of JIS-SCM420, a typical hardened low-alloyed steel. The chemical composition of the material, focusing on both the core and case, was analysed with an optical emission spectrometer (Thermo: ARL 3460). The compositions are compared with those based on JIS G4051: Standard grade SCM 420 [17], as presented in Table 1. A lower amount of molybdenum (Mo) than the standard value of 0.15 may reduce the corrosion resistance and also deteriorate the fatigue resistance of the gear. The specimen prepared for fracture surface analysis was cut from the pinion gear in the transverse cross-section (Fig. 2) and then mounted using a synthetic resin. Later, the specimen was delivered to the metallurgical laboratory to polish and etch using typical procedures. The fracture features, including a fragmented chip of the gear tooth, were analysed using an optical microscope (Olympus laser microscopes: OLS 4000). The characteristics of the fracture surface were examined using a scanning electron microscope (SEM, JOEL: JSM-7800F prime).

Table 1.
Chemical composition of the failed gear and those of SCM 420 steel (%wt.)

Materials	C	Si	Mn	P	S	Ni	Cr	Mo
Failed gear (Case)	0.46	0.32	0.86	0.009	0.012	0.104	0.90	0.15
(Core)	0.21	0.23	0.78	0.016	0.015	0.019	1.035	0.025
JIS-SCM 420	0.18-0.23	0.15-0.35	0.60-0.90	≤ 0.030	≤ 0.030	≤ 0.030	0.90-1.20	0.15-0.25

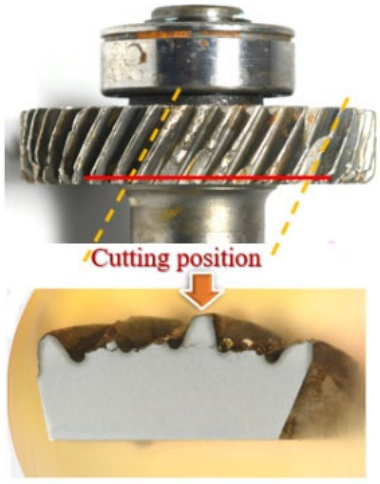

Fig. 2. A investigated cross-sectional area on the failed specimen

2.2. Mechanical testing

A mechanical property was evaluated through Micro hardness testing (ANTON PAAR, MHT-10), utilising an indenter with a diamond pyramid angle of 136 degrees and applying a load of 300 g. To establish a hardness profile according to ASTM E92-82, 10 points on the area of investigation, along the surface to centre for the top land and root and perpendicular with the gear flank, were measured. The interval distance of each point was 0.2 mm.

3. Preliminary stress analysis

In order to estimate the bending and contact stresses of the subjected gear under operating conditions, calculations of bending stress and contact stress are required. Based on the American Gear Manufacturing Association (AGMA) equation [18,19], bending stress can be analysed using the following equation.

$$\sigma_b = \frac{W^t K_o K_v K_s K_H K_B}{b m_t Y_J} \quad (1)$$

where W^t is tangential transmitted load (12.48 kN), K_o is overload factor (1.25), K_s is the size factor (~1), K_H is the load distribution factor (1.16), K_v is a dynamic factor (1.78), $K_B$is the rim-thickness factor (~1), b is the gear face width (22 mm), m_t is the transverse metric module (2.56 mm), and Y_J is the geometric factor for bending strength (0.48).

The safety factor required for bending stress analysis is given by

$$S_F = \frac{S_t Y_N/(K_T K_R)}{\sigma_F} \quad (2)$$

where S_t is the contact strength (450 MPa) [19], Y_N is stress-cycle factor (0.98), K_T is temperature factor (~1), and K_R is reliability factor (~1).

For contact stress analysis [18], the fundamental equation for pitting resistance (contact stress) is:

$$\sigma_c = Z_E \sqrt{\frac{W^t K_o K_v K_s K_H Z_R}{d_{w1} b Z_I}} \quad (3)$$

where Z_E is elastic coefficient (191 N/mm^2), W^t is tangential transmitted load (12.48 kN), K_o is overload factor (1.25), K_s is size factor (~1), K_H is the load distribution factor (1.16), K_v is dynamic factor (1.78), Z_R is the surface condition factor (~1), d_{wl} is the pitch diameter of the pinion (64.80 mm), Z_I is geometry factor (0.16), and b is the gear face width (22 mm).

The safety factor required for contact stress analysis is given by

$$S_H = \frac{S_c Z_N/(K_T K_R)}{\sigma_c} \quad (4)$$

where S_c is the contact strength (1150 MPa) [19], Y_N is a stress-cycle factor (1.1), K_T is temperature factor (~1), and K_R is reliability factor (~1).

4. Finite element (FE) simulation

The helical gear was designed using Computer-Aided Design (CAD) software, facilitating finite element simulation. The simulation was also conducted to estimate bending and contact stresses on the subjected gear tooth. Finally, the simulation results were compared to the calculation results obtained by the AGMA equation.

For the simulation setup, the positions of the pinion gear (red-highlighted area) and drive gear set were defined according to Figure 3. It was assumed that the gears worked under the maximum loading condition. However, based on the actual working conditions, the power of about 144 kW was required for a pick-up truck with a power transmission of 3400 rpm. A pick-up truck power and transmission ratio were also considered to calculate the acting moment on the gears. Boundary conditions, such as power, speed, torque, and elastic coefficient, were set according to 343 N-m load. Ultimately, details regarding the dimensions of the gear tooth and the applicable boundary conditions are documented in Table 2.

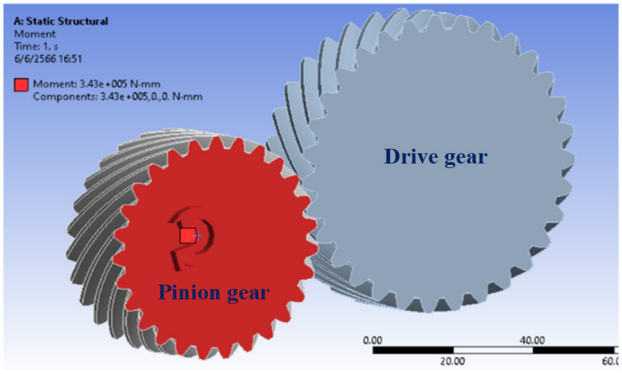

Fig. 3. FE model of the pinion gear and drive gear set

Table 2.
Dimensions and corresponding boundary conditions of the helical gear, related to conventional working conditions

Description	Symbol	Values	Unit
Power	H	144	kW
Speed	n_p	3400	rpm
Torque	τ	343	N-m
Number of teeth pinion gear	N_p	27	teeth
Number of teeth drive gear	N_G	31	teeth
Pinion gear diameter	d_p	60	mm
Drive gear diameter	d_G	80	mm
Normal module	m	2.22	mm
Pressure angle	φ	20°	degree
Helix angle	ψ	30°	degree
Gear face width	b	22	mm
Elastic coefficient	Z_E	191	N/mm^2

Furthermore, FE mesh was generated using tetrahedral elements, as shown in Figure 4. The total number of elements was 635,878, with 1,008,839 nodes. Degrees of Freedom (DOF), only x, y, and z axes, were applied for mesh control. According to the simulation setup, the transmitted loads from the pinion gear were calculated, and the stress distribution was acquired based on the input data [6,20,21].

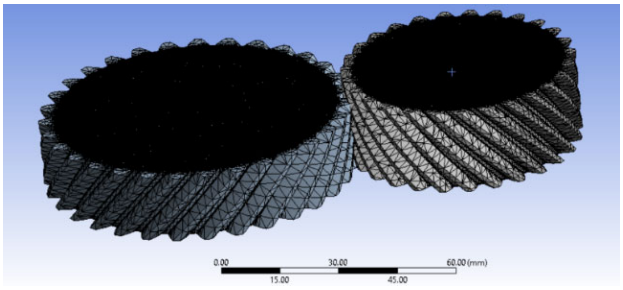

Fig. 4. FE meshing using tetrahedral elements

5. Result and discussion

5.1. Metallographic observation

According to metallographic views, optical micrographs of the helical gear presented in Fig. 5 reveal characteristics of cracks over the cross-sectional gear surface and microstructure obtained at specific locations. The locations were pointed out at a case and core of the corresponding surface, as shown in Figure 5(a). It was found that the gear was broken explicitly with the propagation of cracks within the root of a gear tooth. The crack propagation was found from one side to another. In Figures 5(b) and (c), it is obvious that microstructures of the case and core surfaces implied the influence of microstructure on fatigue crack, especially on the gear tooth (case). The microstructure of the case, at the outer periphery region, could be tempered martensite. It may consist of tiny martensite with uniformly dispersed cementite particles embedded within the ferrite matrix. Tempered martensite formed due to stress relaxation caused by heat treatment. Even though this martensite feature was hard and brittle, it was somewhat softened compared to the feature processed by quenching. This subsequently led to improving ductility and toughness of the gear tooth. The microstructure could be upper bainite for the central region (core). The upper bainite is generally stronger but softened than pearlite; therefore, it exhibits a desirable combination of strength and ductility. The structure revealed fine bainitic laths that were more like pearlite, termed 'feathery' bainite, where a shear mechanism at the austenite grain boundaries nucleated it. These microstructures implied that the gear was heat-treated by carburising, quenching, and tempering. The specific heat treatment is a common practice for SCM 420 steel [22].

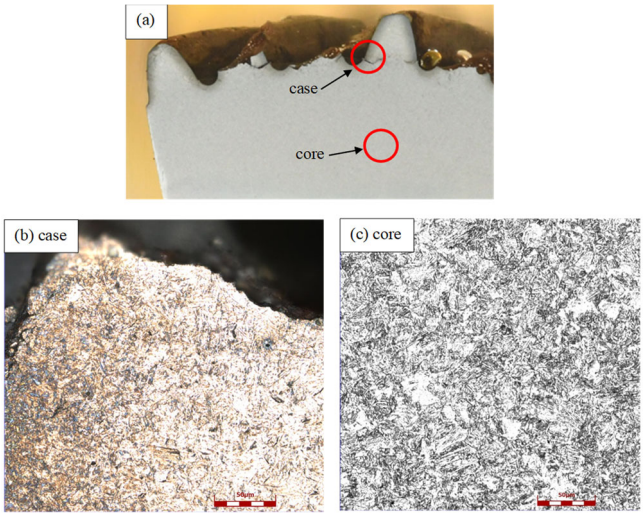

Fig. 5. Optical micrograph of the helical gear showing (a) characteristics of cracks over the crossectional gear surface, (b) 500x magnified case area presented tempered martensite microstructure, (c) 500x magnified core area presented upper bainite microstructure

A low magnification micrograph of a failed gear tooth displayed in Figure 6 indicates a different hardened surface finish on the failed gear tooth. The thickness of the hardened layer was approximately 868 µm. The result of excessive tooth loads resulted in root stresses, which were higher than the endurance limit of the material. When gears were loaded and subjected to adequate repeated stress cycles, the gear tooth failed. Stress risers occasionally exacerbate this condition, subjecting the gear to elevated root stress levels beyond typical predictions. These risers encompass elements such as notches in the root fillet, inclusions, minor heat-treatment cracks, and residual stresses [23].

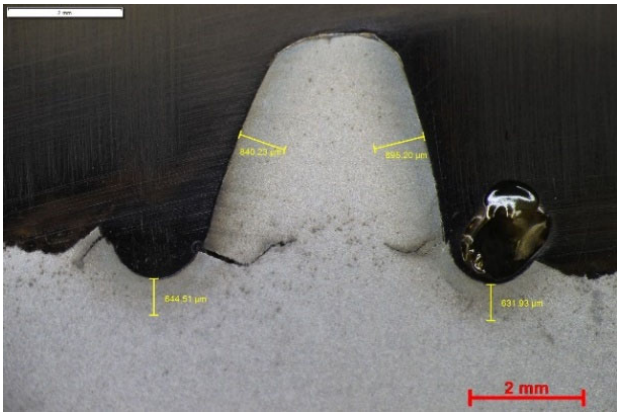

Fig. 6. Different hardened surface layers of the failed gear tooth at 1x magnification

5.2. Fractographic analysis

The failed helical gear is presented in Figure 7. The evaluated area consists of crack origin, ratchet mark, and final overload zone. From a morphological aspect, it can be concluded that the failure was initiated at the crack origin and then propagated into the centre. The propagation of crack origin caused the formation of ratchet marks. The ratchet marks presented on the fracture surface indicate that the fracture had multiple origins. The ratchet mark could be due to high stress exerted on the workpiece or the area of high-stress concentration. Eventually, the crack reached the point where the remaining material was overstressed, forming the final overload zone [24].

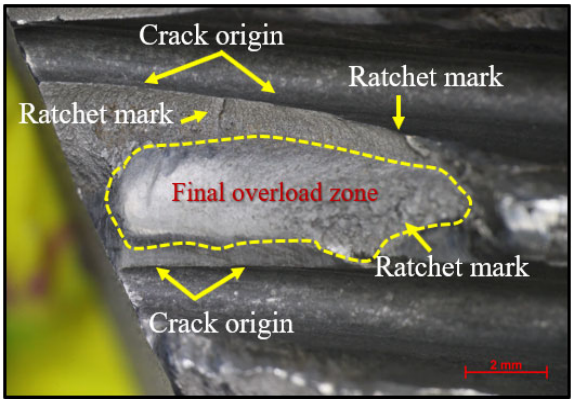

Fig. 7. The cracking characteristics of the failed helical gear

The location of a rachet mark on the failed gear is presented in Fig. 8 (a). It is indicated that the rachet mark propagated perpendicularly from the tip edge or crack initiation zone to the instant fracture zone. Several small cracks formed near the rachet marks were found at higher magnifications, as shown in Fig. 8 (b). In Fig. 8 (c) and (d), the intergranular fracture was presented along a triple junction of grain boundaries. This feature may result from a brittleness of grain structure, leading to increased mechanical properties of the hardened material [25].

A fractograph shown in Figure 9(a) reveals a fracture tip in the area of the instant fracture zone. It is noteworthy that the ductile fracture was found in the vicinity of the font tip (Fig. 9(b)). This area has high magnification (Fig. 9(c-d)), ductile dimples were formed. The formation of dimples is characteristic of ductile fracture resulting from uniaxial tensile failure. Each dimple developed from micro-voids and subsequently propagated to fracture. Noticeably, the dimples were distorted and formed on 45 angles of the shear lip. A group of dimple distortions assembled into a parabolic C-shape. This specific shape may indicate shear failure, a fracture mode of ductile failure arising from shear load [26].

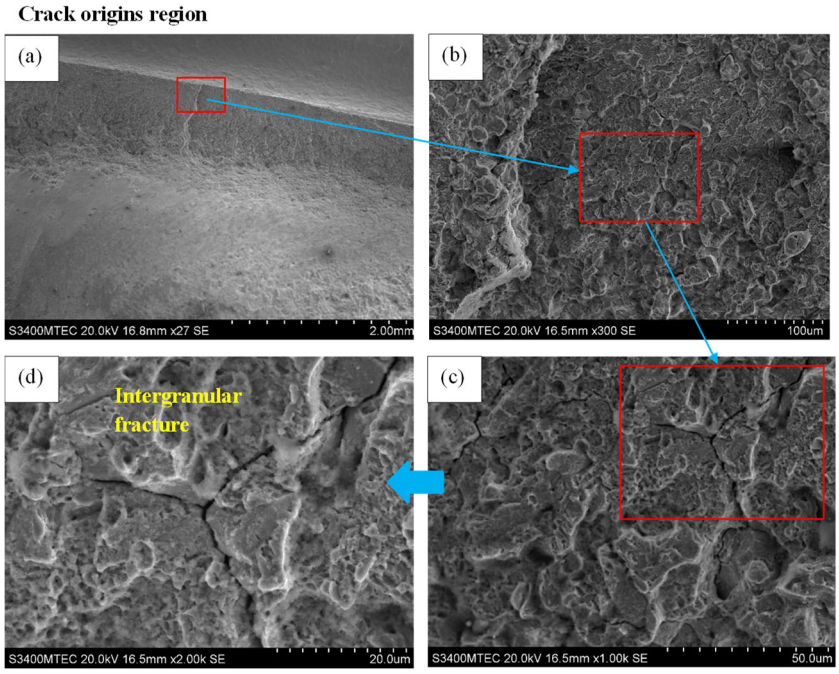

Fig. 8. SEM fractographs showing (a) The failed gear outer surface region fracture at 30x magnification, (b) the formation of small cracks near rachet marks at 300x magnification, (c-d) characteristic of intergranular fracture along a triple junction of grain boundaries at 1.00 kx and 2.00 kx magnifications, respectively

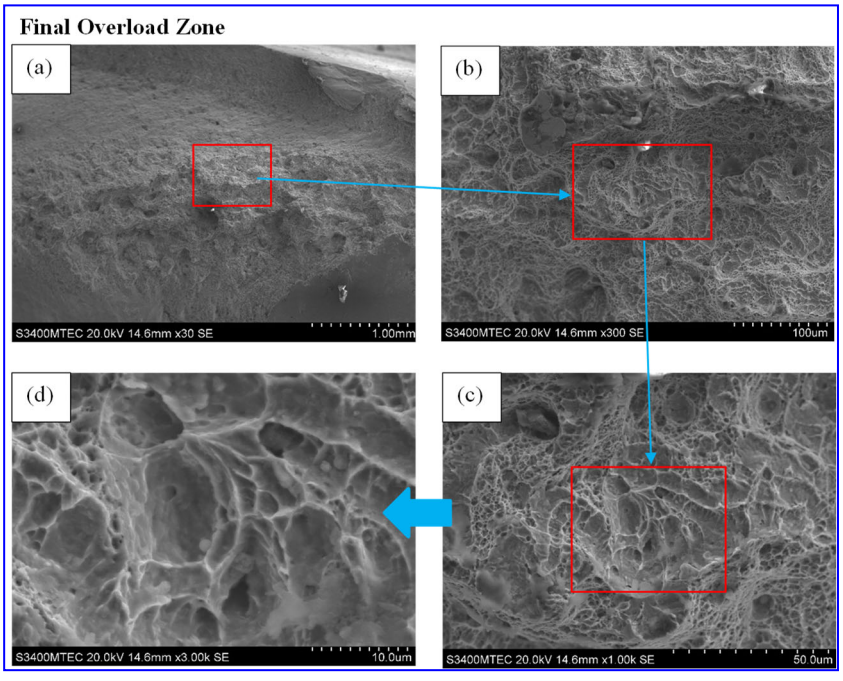

Fig. 9. SEM fractography showing (a) a fracture tip in the area of the instant fracture zone at 30x magnification, (b) characteristic of ductile fracture in the vicinity of the fracture font tip at 300x magnification, (c-d) formations of dimples into a parabolic C-shape at 1.00 kx and 3.00 kx magnifications, respectively

5.3. Mechanical property

According to Figure 10, hardnesses were measured along three cross-sectional areas: the tip circle (green arrow), reference circle (red arrow), and root circle (blue arrow). The hardness distribution profiles obtained across these areas are displayed in Figure 11.

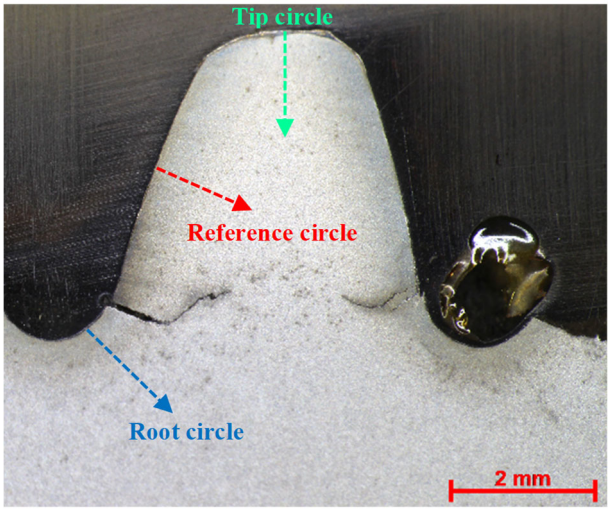

Fig. 10. Hardness measured areas on the failed helical gear

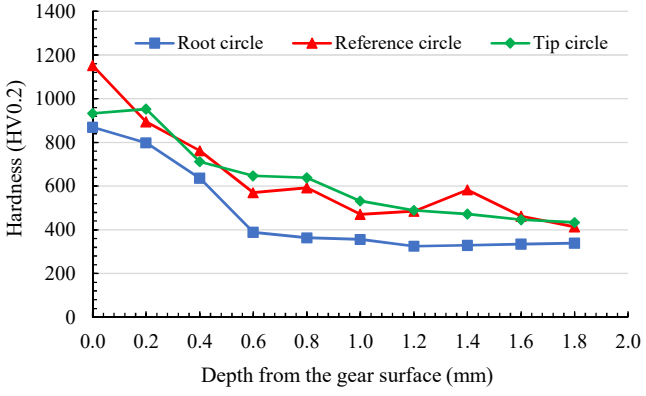

Fig. 11. Hardness distribution profiles obtained across the measured layers of the failed helical gear

Decreasing in hardness values depended on the hardening depth from the gear surface. The maximum values obtained at the tip, reference, and root circle were 933 HV, 1152.57 HV, and 870 HV, respectively. Meanwhile, the minimum values measured at the tip circle, reference circle, and root circle were 434 HV, 414 HV, and 339 HV, respectively. The maximum values of all profiles were explicitly found at the outer surface (case), whereas the minimum values were raised at areas towards the gear centre (core). The results show that the hardness values of some areas of the gear were somewhat different depending on the hardening depth. It was because of the effect of heat treatment caused by carburising and hardening treatments. The tempering process might be a major cause of gear failure [27].

5.4. Simulation results

Based on the preliminary stress analysis, the calculated bending stress (σ_b) was 1191.51 MPa, and the safety factor (S_F) was 0.37. It was found that the calculated bending stress was higher than the bending strength of the gear material, which was 450 MPa [22]. Similar to references [6,20,21,28,29], the bending strength of the chromium molybdenum steel SCM 420 is about 450 MPa. It indicates that the calculated bending stress from general operation was 2.65 times higher than the allowable bending strength. For the calculated contact stress, the value (σ_c) was 2269.74 MPa, and the safety factor (S_H) was 0.751. From a reference [19], the contact strength of the material is 1550 MPa. Thus, the stress obtained from the calculation was also somewhat higher than the material strength.

For the simulation results, stress distributions over the simulated results can be seen in Figures 12 and 13. In contrast, the deformation gradient on a simulated result can be visible in Figure 14. The maximum principal stress was 1194.9 MPa, which was close to the calculated bending stress. The bending stress values increased with increasing torque. The increased values were in close agreement with those obtained from the AGMA equation. According to Figure 13, the maximum equivalent stress was 2266.7 MPa, located near the tangential transmitted load. Such a value at the highest-stress density area was 12.48 kN. The simulated result was closely related to contact stress obtained from the calculated result. The contact stress started from the surface of a gear tooth. The bending stress was developed toward the central axis of the gear. The development of bending stress could lead to the formation of the contact stress. Hence, the final fracture occurs when the torque exceeds the contact strength of 1550 MPa [19]. The calculated contact stress due to general operation was 1.46 times higher than the allowable contact strength.

In Figure 14, the total deformation was 0.29813 mm, and Figure 15 shows the distribution of safety factors. The minimum value of 2.80 was presented on an oblique angle of the gear tooth. The calculated and FE simulation results are very similar [6,20,21,28,29].

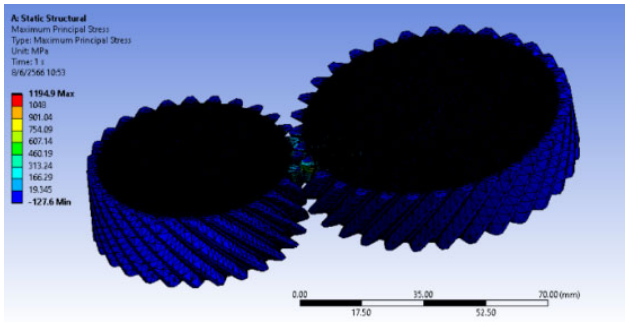

Fig. 12. Distributions of maximum principal stress on the Finite Element (FE) model

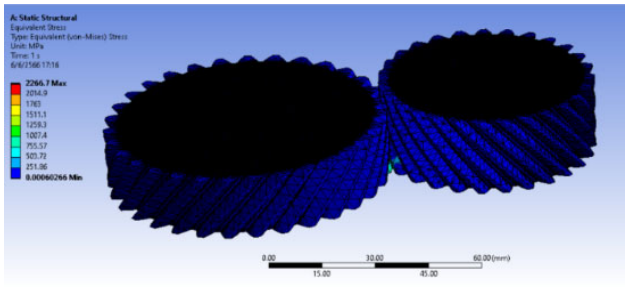

Fig. 13. Distributions of equivalent Von Mises stress on the Finite Element (FE) model

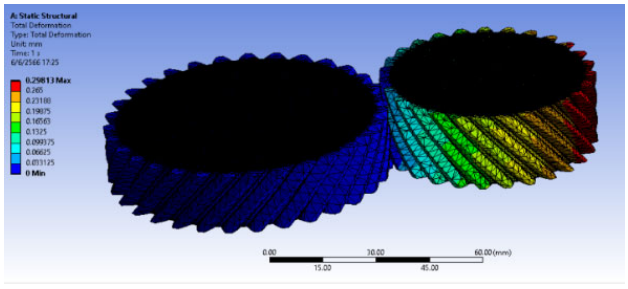

Fig. 14. Distributions of total deformation on the Finite Element (FE) model

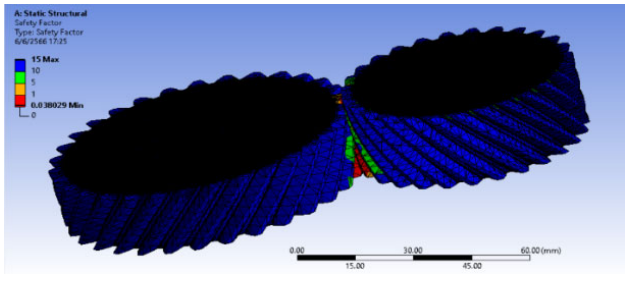

Fig. 15. Distributions of safety factors on the Finite Element (FE) model

6. Conclusions

This research investigated the root cause of failure in the 4th gear of a pick-up truck. Fracture on the failed helical gear was characterised through metallographic and fractographic analyses. Mechanical testing and finite element simulation were employed to assess the factors contributing to the gear failure. The results of the experiments and simulations can be concluded as follows.

1. Metallographic investigations revealed cracks on the case and core of the gear tooth. The hardened layer of the specimen was approximately 868 µm depth. The microstructure observed in the case layer was martensite, leading to a hard and brittle surface due to the carburising process.
2. Fractographic examinations indicated that the failure initiated at the crack origins and then propagated to the instant fracture zone in the core of the gear tooth. Multiple crack origins accelerated the development of ratchet marks, attributed to the high intensity of stress exerted on the workpiece. Ultimately, this led to a substantial final overload zone.
3. Maximum hardness values measured at the reference circle, tip circle, and root circle were 1152.57 HV, 933 HV and 870 HV, respectively. Hardness decreased with increasing depth of the gear surface due to the effects of carburising and hardening treatments.
4. Stress is initiated from the contact stress on the gear tooth surface and transformed into bending stress along the central axis of the gear. The contact stress became critical when the torque surpassed the contact strength of the material. The value was approximately 1550 MPa. Both the calculated contact stress and the finite element analysis exceeded the contact strength of the gear material by 1.46 times. Such an exceed value ultimately led to the eventual fracture of the gear.

Research funding

This research was supported the funding source by Rajamangala University of Technology Krungthep (RMUTK).

Authors contribution

Design the experiments and formal analysis – P. Janmanee and K. Utjimajiratthitikarn; writing-original draft preparation – P. Janmanee and K. Utjimajiratthitikarn; graphical design

and analysed – C. Thanadngarn and R. Saodaen; writing-review and editing – T. Kumnorkaew and K. Jamkamon; supervisor – P. Janmanee; project administration – K. Utjimajiratthitikarn.

Acknowledgements

The research was supported by the Mechanical and Industrial Engineering Department, Faculty of Engineering, Rajamangala University of Technology for research equipment and facilities. The authors express thanks to the National Metal and Materials Technology Center (MTEC) for providing help and guidance on experiments and simulations.

References

[1] A.M. Heyes, Automotive component failure, Engineering Failure Analysis 5/2 (1998) 129-141. DOI: https://doi.org/10.1016/S1350-6307(98)00010-7

[2] O. Hrevtsev, N. Selivanova, P. Popovych, L. Poberezhny, V. Sakhno, O.Shevchuk, L. Poberezhna, I. Murovanyi, A. Hrytsanchuk, O. Romanyshyn, Simulation of thermomechanical processes in disc brakes of wheeled vehicles, Journal of Achievements in Materials and Manufacturing Engineering 104/1 (2021) 11-20.
DOI: https://doi.org/10.5604/01.3001.0014.8482

[3] O. Hrevtsev, N. Selivanova, P. Popovych, L. Poberezhny, V.Ya. Brych, Yu. Rudyak, O. Shevchuk, N. Bakulina, R. Rozum, M. Buriak, Stress-strain state simulation of non-uniformly heated elements of components and assemblies of automotive, Journal of Achievements in Materials and Manufacturing Engineering 115/1 (2022) 26-32.
DOI: https://doi.org/10.5604/01.3001.0016.2339

[4] L.-H. Zhao, Q.-K. Xing, J.-Y. Wang, S.-L. Li, S.-L. Zheng, Failure and root cause analysis of vehicle drive shaft, Engineering Failure Analysis 99 (2019) 225-234. DOI: https://doi.org/10.1016/j.engfailanal.2019.02.025

[5] B. Karpuschewski, M. Beutner, J. Eckebrecht, J. Heinzel, T. Husemann, Surface integrity aspects in gear manufacturing, Procedia CIRP 87 (2020) 3-12. DOI: https://doi.org/10.1016/j.procir.2020.05.112

[6] R.S. Miranda, C. Cruz, N. Cheung A.P.A. Cunha, Fatigue Failure Analysis of a Speed Reduction Shaft, Metals 11/6 (2021) 856.
DOI: https://doi.org/10.3390/met11060856

[7] V. Handikherkar, S. Dhangar, S. Patil, V.M. Phalle, Stress Analysis of Parallel Misaligned Spur Gear Pair, Proceedings of the International Conference on Advances in Thermal Systems, Materials and Design Engineering "ATSMDE2017", Mumbai, India, 2017, 1-7.

[8] A. Shehata, M.A. Adnan, O.D. Mohammed, Modeling the effect of misalignment and tooth microgeometry on helical gear pairs in mesh, Engineering Failure Analysis 106 (2019) 104190.
DOI: https://doi.org/10.1016/j.engfailanal.2019.104190

[9] M. Molaie, F.S. Samani, F. Pellicano, Spiral Bevel Gears Nonlinear Vibration Having Radial and Axial Misalignments Effects, Vibration 4/3 (2021) 666-678.
DOI: https://doi.org/10.3390/vibration4030037

[10] P.J.L. Fernandes, C. McDuling, Surface contact fatigue failures in gears, Engineering Failure Analysis 4/2 (1997) 99-107. DOI: https://doi.org/10.1016/S1350-6307(97)00006-X

[11] P.J.L. Fernandes, Tooth bending fatigue failures in gears, Engineering Failure Analysis 3/3 (1996) 219-225. DOI: https://doi.org/10.1016/1350-6307(96)00008-8

[12] K. Kishore, A. Sharma, G. Mukhopadhyay, Failure Analysis of a Gearbox of a Conveyor Belt, Journal of Failure Analysis and Prevention 20 (2020) 1237-1243.
DOI: https://doi.org/10.1007/s11668-020-00928-4

[13] H. Liu, H. Liu, C. Zhu, R.G. Parker, Effects of lubrication on gear performance: A review, Mechanism and Machine Theory 145 (2020) 103701. DOI: https://doi.org/10.1016/j.mechmachtheory.2019.103701

[14] D.K. Pandey, H.-C. Lim, Pinion Failure Analysis of a Helical Reduction Gearbox in a Kraft Process, Applied Sciences 10/8 (2020) 2935.
DOI: https://doi.org/10.3390/app10082935

[15] C.O.F.T, Ruchert, C.I.S. Maciel, A.E.A. Chemin, Sub case origin fatigue in teeth of helical gear of a TA 67n turbo reducer, Engineering Failure Analysis 108 (2020) 104286.
DOI: https://doi.org/10.1016/j.engfailanal.2019.104286

[16] F. Zhao, X. Ding, X. Fan, R. Cui, Y. Li, T. Wang, Contact fatigue failure analysis of helical gears with non-entire tooth meshing tests, Metals 8/9 (2018) 693.
DOI: https://doi.org/10.3390/met8090693

[17] W. Feng, Z. Feng, L. Mao, Failure analysis of a secondary driving helical gear in transmission of electric vehicle, Engineering Failure Analysis 117 (2020) 104934. DOI: https://doi.org/10.1016/j.engfailanal.2020.104934

[18] Q. Xiaofeng, L. Jie, Z. Xingguo, F. Li, P. Ruiqiang, Fracture failure analysis of transmission gear shaft in a bidirectional gear pump, Engineering Failure Analysis 118 (2020) 104886.
DOI: https://doi.org/10.1016/j.engfailanal.2020.104886

[19] W.D. Callister Jr., Materials science and engineering an introduction. 7th Edition, John Wiley and Sons, New York, 2007.
[20] Japanese Steels and Alloys, Japanese steel grading – SCM Grades – SCM420. Available from: http://steeljis.com/jis_steel_datasheet.php?name_id=15
[21] Z. Yu, X. Xu, Failure investigation of a truck diesel engine gear train consisting of crankshaft and camshaft gears, Engineering Failure Analysis 17/2 (2010) 537-545. DOI: https://doi.org/10.1016/j.engfailanal.2009.10.003
[22] L. Zheng, T. Yang, S. Xue, G. Li, X. Liu, Fracture failure analysis of the teeth of conjunction gear made of 20MnCr5S steel, Engineering Failure Analysis 134 (2022) 106006. DOI: https://doi.org/10.1016/j.engfailanal.2021.106006
[23] R. Budynas, K. Nisbett, Shigley's Mechanical Engineering Design, 10th Edition, McGraw-Hill, New York, 2014.
[24] S.R. Schmid, B.J. Hamrock, B.O. Jacobson, Fundamentals of Machine Elements, 3rd Edition, CRC Press, Boca Raton, 2014.
[25] P. Kulkarni, H. Yaragudri, M.A. Umarfarooq, Contact Stress Analysis and Optimization of Bevel Gear Pairs by Theoretical and FEA, International Journal of Latest Technology in Engineering, Management and Applied Science 6/8 (2017) 112-121.
[26] V. Boonmag, A. Phukaoluan, O. Wisesook, G. Pluphrach, Comparison of Bending Stress and Contact Stress of Helical Gear Transmission Using Finite Element Method, International Journal of Mechanical Engineering and Robotics Research 8 (2019) 99-103. DOI: https://doi.org/10.18178/ijmerr.8.1.99-103
[27] G. Vukelica, D. Pastorcicb, G. Vizentina, Z. Bozicc, Failure investigation of a crane gear damage, Engineering Failure Analysis 115 (2020) 104613. DOI: https://doi.org/10.1016/j.engfailanal.2020.104613
[28] M. Wiater, G. Chladek, J. Żmudzki, FEM numerical simulation of contact stresses between driving shaft and hub impeller of fuel pump, Journal of Achievements in Materials and Manufacturing Engineering 113/1 (2022) 13-21. DOI: https://doi.org/10.5604/01.3001.0016.0941
[29] G. Popov, V. Zubanov, E. Goriachkin, A. Scherban, A.A. Shvyrev, Verification of a Numerical Model of a Two-Stage HPT of a Modern GTE for Civil Aviation, International Journal of Mechanical Engineering and Robotics Research 12/2 (2023) 78-83. DOI: https://doi.org/10.18178/ijmerr.12.2.78-83